Dept. of Math. University of Oslo
Mechanics and Applied Mathematics
No. 1
ISSN 0809–4403 September 2005

IMPLEMENTATION OF NON-LINEAR ADVECTION TERMS IN A HIGH RESOLUTION TIDAL MODEL

Karina Hjelmervik[(1)], Atle Ommundsen[(2)], Bjørn Gjevik[(1)]

(1) Department of Mathematics, University of Oslo, Norway

(2) Norwegian Defence Research Establishment, Kjeller, Norway

Abstract

Various methods for approximating the non-linear advection terms in a high resolution tidal model with complex coastal boundaries have been implemented and tested. The model, driven by the dominant M_2 tidal component at the open boundaries, has been applied to a model domain with 100 meter grid resolution for the Tjeldsundet channel in northern Norway. Overtides, intensivated jets and eddy structures appear in the current fields of the full non-linear simulations. How these flow features depend on the way the friction terms are calculated and the way the non-linear advection terms are calculated in a zone near the coastal boundaries, are discussed. Some comparison with field measurements have also been made.

1 Introduction

In the papers by Moe et al. (2002) and Moe et al. (2003) the tides in two regions on the western and northern coast of Norway were simulated with a high resolution numerical model with horizontal grid size of 500 meters. The first version of this model was developed in the early 1990s and used for simulations of the tides in the Norwegian and Barents Seas (Gjevik (1990), and Gjevik et al. (1994)). In this model the non-linear advection terms were neglected, but the non-linear bottom friction was retained. Also a non-linear representation of the horizontal eddy viscosity was adapted (Smagorinsky (1963)). For this reason we shall refer to this model as the partially linearized

numerical model (PLN-model). More recently an upgraded version of the model has been used for simulation of the tide in the outer Trondheimsfjord with a horizontal grid resolution of 50 and 100 meters (Gjevik et al. (2004)).

In narrow straights and channels with strong tidal currents it is well known that non-linear effects can lead to significant distortion of the tides. In these cases the non-linear advections terms must clearly be included. This is for example the case, among many others, in the Tjeldsund and Ramsund channels east of The Lofoten Islands in northern Norway. These channels connect the Vestfjord and the Ofotfjord with the Vågsfjord in Vesterålen and are important sailing lanes for coastal traffic. In an attempt to model the tidal currents in these channels, with a horizontal grid resolution of 25-50 meters, the non-linear terms have to be included. The challenge is to find robust and accurate numerical schemes which are stable, even with complex coastlines and bottom topography, without introducing too strong smoothing or damping of the current fields.

This report discusses, in details, several methods for including the non-linear advection terms in the original PLN-model. As an example the model is set up for Tjeldsund and Ramsund channels and the results of these simulations are used to demonstrate how the simulated tidal currents are affected by the different implementations of the non-linear advection terms. Martinsen and Engedahl (1987)

2 Model equations

The depth-integrated shallow water equations in a Cartesian coordinate system (x,y,z) with the x- and y-axis horizontal in the level of the undisturbed surface, are given by:

$$\frac{\partial \eta}{\partial t} = -\frac{\partial U}{\partial x} - \frac{\partial V}{\partial y} \tag{1}$$

$$\frac{\partial U}{\partial t} + \frac{\partial}{\partial x}(\frac{U^2}{H}) + \frac{\partial}{\partial y}(\frac{UV}{H}) - fV = -gH\frac{\partial \eta}{\partial x} + F^x + A^x \tag{2}$$

$$\frac{\partial V}{\partial t} + \frac{\partial}{\partial x}(\frac{UV}{H}) + \frac{\partial}{\partial y}(\frac{V^2}{H}) + fU = -gH\frac{\partial \eta}{\partial y} + F^y + A^y \tag{3}$$

where (U, V) are the components of volume flux vector per unit length in the horizontal plane, η the vertical displacement of the sea surface from the mean sea level, $H = H_0 + \eta$ the total depth, H_0 the mean depth, g the acceleration of gravity, and f the Coriolis parameter.

The bottom friction terms, F^x and F^y, are given by:

$$F^x = -c_D \frac{U}{H} \frac{\sqrt{U^2+V^2}}{H} \tag{4}$$

$$F^y = -c_D \frac{V}{H} \frac{\sqrt{U^2+V^2}}{H} \tag{5}$$

where c_D is the drag coefficient of the quadratic bottom shear stress. The horizontal eddy viscosity terms, A^x and A^y, are given by:

$$A^x = \nu \nabla^2 U \tag{6}$$

$$A^y = \nu \nabla^2 V \tag{7}$$

where ν is the eddy viscosity coefficient of the horizontal shear stress.

For the eddy viscosity coefficient the Smagorinsky model (Smagorinsky (1963)) is adapted:

$$\nu = ql^2[(\frac{\partial \overline{u}}{\partial x})^2 + \frac{1}{2}(\frac{\partial \overline{u}}{\partial y} + \frac{\partial \overline{v}}{\partial x})^2 + (\frac{\partial \overline{v}}{\partial y})^2]^{\frac{1}{2}} \tag{8}$$

where q is a constant, l is a length scale which is set equal to the grid size, and $(\overline{u}, \overline{v})$ denote the components of the depth mean current velocity defined to the first order by:

$$\overline{u} = \frac{U}{H}, \qquad \overline{v} = \frac{V}{H}$$

With q=0.1, a grid size of 100 meters, and a current speed of the order 1 m/s, eq. (8) leads to an eddy viscosity of the order 10 m^2/s. In some simulations a constant horizontal eddy viscosity with ν ranging from 1 to 10 m^2/s is applied instead of the flow dependent viscosity in eq. (8).

By neglecting the non-linear advection terms and the horizontal shear stress, the shallow water eqs. (1) to (3), simplify to the following:

$$\frac{\partial \eta}{\partial t} = -\frac{\partial U}{\partial x} - \frac{\partial V}{\partial y} \tag{9}$$

$$\frac{\partial U}{\partial t} - fV = -gH_0 \frac{\partial \eta}{\partial x} - c_D \frac{U}{H_0} \frac{\sqrt{U^2+V^2}}{H_0} \tag{10}$$

$$\frac{\partial V}{\partial t} + fU = -gH_0 \frac{\partial \eta}{\partial y} - c_D \frac{V}{H_0} \frac{\sqrt{U^2+V^2}}{H_0} \tag{11}$$

This is the same set of equations as implemented in the PLN-model. The equations were discretized on a C-grid (Mesinger and Arakawa (1976)) shown

in figure 1, with a uniform spatial grid resolution $\triangle s$ and time step $\triangle t$:

$$\frac{\eta_{i,j}(t+\triangle t)-\eta_{i,j}(t)}{\triangle t} = -\frac{U_{i+1,j}(t)-U_{i,j}(t)}{\triangle s}-\frac{V_{i,j+1}(t)-V_{i,j}}{\triangle s} \quad (12)$$

$$\frac{U_{i,j}(t+\triangle t)-U_{i,j}(t)}{\triangle t} = f\overline{V}_{i,j}(t)-g\overline{H_0}^{i}_{i,j}\frac{\eta_{i,j}(t+\triangle t)-\eta_{i-1,j}(t+\triangle t)}{\triangle s} - c_D\frac{U_{i,j}(t)}{\overline{H_0}^{i}_{i,j}}\frac{\sqrt{{U_{i,j}}^2(t)+{\overline{V}_{i,j}}^2(t)}}{\overline{H_0}^{i}_{i,j}} \quad (13)$$

$$\frac{V_{i,j}(t+\triangle t)-V_{i,j}(t)}{\triangle t} = -f\overline{U}_{i,j}(t+\triangle t)-g\overline{H_0}^{j}_{i,j}\frac{\eta_{i,j}(t+\triangle t)-\eta_{i,j-1}(t+\triangle t)}{\triangle s} - c_D\frac{V_{i,j}(t)}{\overline{H_0}^{j}_{i,j}}\frac{\sqrt{{\overline{U}_{i,j}}^2(t+\triangle t)+{V_{i,j}}^2(t)}}{\overline{H_0}^{j}_{i,j}} \quad (14)$$

where

$$\begin{aligned}
\overline{H_0}^{i}_{i,j} &= \frac{1}{2}(H_{0i,j}+H_{0i-1,j}) \\
\overline{H_0}^{j}_{i,j} &= \frac{1}{2}(H_{0i,j}+H_{0i,j-1}) \\
\overline{V}_{i,j} &= \frac{1}{4}(V_{i,j}+V_{i-1,j}+V_{i,j+1}+V_{i-1,j+1}) \\
\overline{U}_{i,j} &= \frac{1}{4}(U_{i,j}+U_{i+1,j}+U_{i,j-1}+U_{i+1,j-1})
\end{aligned}$$

The simulations are started from rest (η=U=V=0) and are driven by specified surface elevation η at the open boundaries. Boundary values are either obtained from a model covering a larger domain or by interpolating data from a model with coarses grid. The interior solution are adjusted to the specified boundary conditions with the flow relaxation scheme (*FRS*), Martinsen and Engedahl (1987). The *FRS* softens the transition from an exterior solution to an interior solution by use of a grid zone where the two solutions dominate at each ends respectively. How a FRS zone can be implemented in tidal models is described by Moe et al. (2002) and Moe et al. (2003). Further details about the PLN-model, are given in the same papers.

3 Implementation of non-linear terms

3.1 The total depth

The first and easiest modification of the PLN-model is to use the total depth, H, instead of the mean depth, H_0. This is done by adding η to H_0 after η

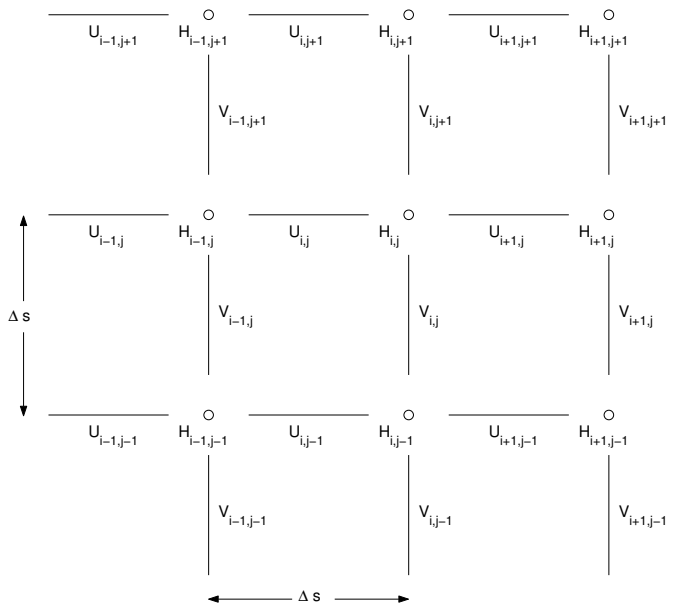

Figure 1: *C-grid stensil with a uniform spatial grid resolution* $\triangle s$*. The circles denotes grid points where both sea surface displacement,* η*, and depth,* H*, are specified. Lines represent grid nodes for volume fluxes* U *and* V*.*

is calculated in every grid node, and then using H in the calculations for U and V.

In order to study the effect of replacing H_0 by $H = H_0 + \eta$ in the PLN-model, eqs. (12)-(14), some numerical tests have been made, see section 5.1.

3.2 The non-linear advection terms

Following the same discretization as used in the linear equations, the non-linear advection terms in eqs. (2) and (3) have been represented with the numerical form:

$$N^x_{i,j} = \frac{1}{\triangle s}\left(\frac{\overline{U}^i_{i,j}{}^2}{H_{i,j}} - \frac{\overline{U}^i_{i-1,j}{}^2}{H_{i-1,j}}\right) + \frac{1}{\triangle s}\left(\frac{\overline{U}^j_{i,j+1}\overline{V}^i_{i,j+1}}{\overline{H}_{i,j+1}} - \frac{\overline{U}^j_{i,j}\overline{V}^i_{i,j}}{\overline{H}_{i,j}}\right) \tag{15}$$

$$N^y_{i,j} = \frac{1}{\triangle s}\left(\frac{\overline{U}^j_{i+1,j}\overline{V}^i_{i+1,j}}{\overline{H}_{i+1,j}} - \frac{\overline{U}^j_{i,j}\overline{V}^i_{i,j}}{\overline{H}_{i,j}}\right) + \frac{1}{\triangle s}\left(\frac{\overline{V}^j_{i,j}{}^2}{H_{i,j}} - \frac{\overline{V}^j_{i,j-1}{}^2}{H_{i,j-1}}\right) \tag{16}$$

where

$$\overline{U}^i_{i,j} \;=\; \frac{1}{2}(U_{i+1,j} + U_{i,j})$$

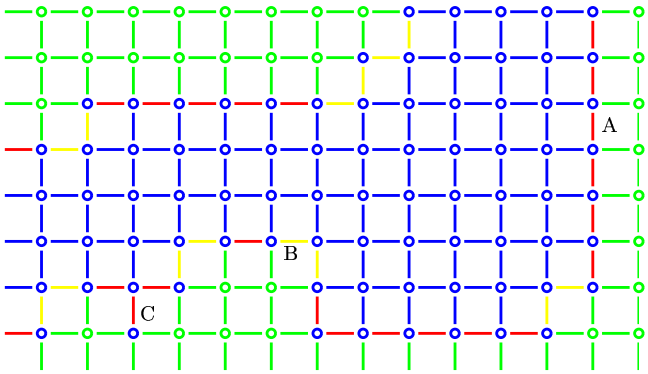

Figure 2: *Example of the grid mesh in the coastal zone. Red and yellow lines illustrate fluxes in the coastal zone, blue in the interior domain. Blue circles represent points for sea surface displacement. Green circles represent land points.*

$$
\begin{aligned}
\overline{U}^{j}_{i,j} &= \frac{1}{2}(U_{i,j} + U_{i,j-1}) \\
\overline{V}^{i}_{i,j} &= \frac{1}{2}(V_{i,j} + V_{i-1,j}) \\
\overline{V}^{j}_{i,j} &= \frac{1}{2}(V_{i,j+1} + V_{i,j}) \\
\overline{H}_{i,j} &= \frac{1}{4}(H_{i,j} + H_{i-1,j} + H_{i,j-1} + H_{i-1,j-1})
\end{aligned}
$$

For the nearest fluxes parallel to the coastline we have used a one-sided difference in the non-linear advection terms. These fluxes are said to be located in a *coastal zone* as illustrated in figure 2.

To include the non-linear advection terms also for the coastal zone, approximation methods must be used. The four approximation methods used for a straight coastline are illustrated by figure 3:

1. The non-linear advection terms in the coastal zone, $f(0)$, are set to zero:

$$f_1(0) = 0$$

2. The non-linear advection terms in the coastal zone, $f(0)$, equal the non-linear advection terms in the the nearest neighbouring grid cell, $f(1)$:

$$f_2(0) = f(1)$$

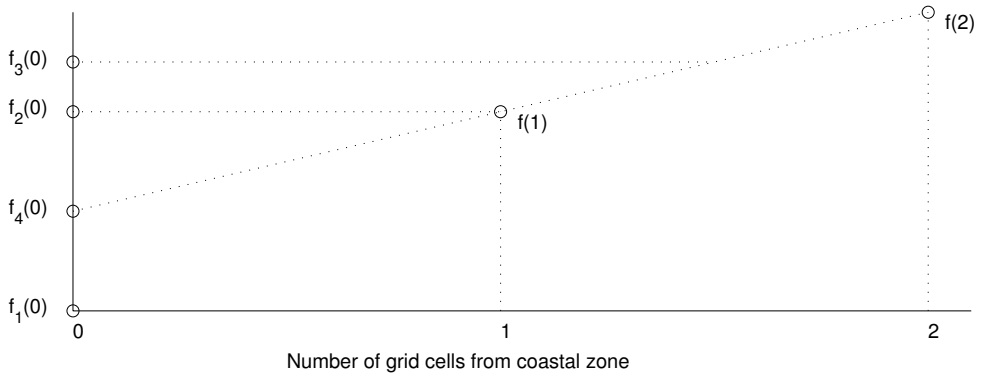

Figure 3: *Four methods to approximate a non-linear advection term in the coastal zone, $f_n(0)$, where n=1,2,3,4 represents the method listed in the text. $f(1)$ is the value of the term one grid cell away from the coastal zone, and $f(2)$ the value two grid cells away from the coastal zone.*

3. The non-linear advection terms in the coastal zone, $f(0)$, equal the mean of the value of the terms in two grid points nearest to the coast, $f(1)$ and $f(2)$:

$$f_3(0) = \frac{1}{2}(f(1) + f(2))$$

4. The non-linear advection terms in the coastal zone, $f(0)$, is determined by a linear extrapolation of the non-linear advection terms from two grid cells close to the coast, $f(1)$ and $f(2)$:

$$f_4(0) = f(1) + \frac{f(2) - f(1)}{2 - 1}(0 - 1) = 2f(1) - f(2)$$

The following describe in detail how the four methods were modified in case of more complicated coastlines:

3.2.1 Special case: channel

In a narrow channel with only one or two grid cells, the non-linear advection terms are set to zero as shown in figure 4.

In a channel with three grid cells, only the non-linear advection terms in the middle of the channel are calculated without one-sided differences. The non-linear advection terms in the coastal zone on each side of the channel, may be approximated using only the non-linear advection terms in the middle of the channel. This is indicated with '1' in figure 4.

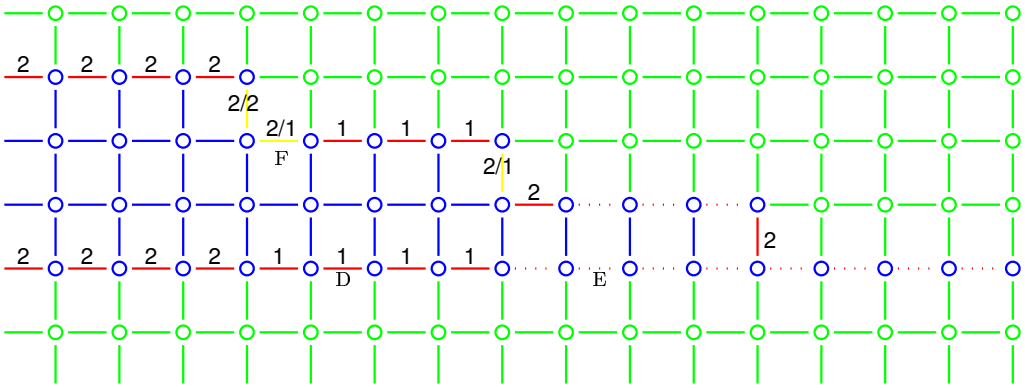

Figure 4: *Example of a narrow channel. Red and yellow lines illustrate fluxes located in the coastal zone, blue in the interior domain. Dotted lines illustrates fluxes where the non-linear advection terms are set to zero. Blue circles represent points for sea surface displacement. Green circles represent land points.*

If the non-linear advection terms in a coastal zone are approximated using two or more non-linear advection terms in one direction, this in indicated with '2' in figure 4.

3.2.2 Special case: corners

A flux is said to be in the coastal zone *near a corner* if the parallel neighbouring fluxes in two directions is located in the water outside the coastal zone.

The non-linear advection term for a flux in the coastal zone near a corner is approximated as the mean value of the approximation in these directions.

The flux marked with '2/2' in figure 4 and all the fluxes illustrated by yellow lines in figure 2 may use two non-linear advection terms in each direction to approximate the non-linear advection term in the coastal zone.

The fluxes marked with '2/1' in figure 4 may use two non-linear advection terms in one direction and one term in another direction to approximate the terms in the coastal zone.

3.2.3 Implementation of the non-linear advection terms

Before expressing the full equations for the non-linear advection terms, four new parameters are defined[1]. $Z^x_{i,j}$ and $Z^y_{i,j}$ denote whether the fluxes are

[1]Note that Z^x is called uinl in the model code, Z^y is called vinl, C^x is called uik, and C^y is called vik.

located in the coastal zone or in the interior domain:

$$Z^x_{i,j} = \begin{cases} 0, & \text{if the flux } U_{i,j} \text{ lies in the coastal zone or next to a land node} \\ 1, & \text{if the flux } U_{i,j} \text{ lies in the water outside the coastal zone} \end{cases}$$

$$Z^y_{i,j} = \begin{cases} 0, & \text{if the flux } V_{i,j} \text{ lies in the coastal zone or next to a land node} \\ 1, & \text{if the flux } V_{i,j} \text{ lies in the water outside the coastal zone} \end{cases}$$

and $C^x_{i,j}$ and $C^y_{i,j}$ denote the coast type for the fluxes in the coastal zone:

$$C^x_{i,j} = \begin{cases} 0, & \text{if the flux } U_{i,j} \text{ lies in the water outside the coastal zone} \\ & \text{or next to a land node} \\ 1, & \text{if the flux } U_{i,j} \text{ lies in a coastal zone, but not near a corner} \\ 0.5, & \text{if the flux } U_{i,j} \text{ lies in a coastal zone near a corner} \end{cases}$$

$$C^y_{i,j} = \begin{cases} 0, & \text{if the flux } V_{i,j} \text{ lies in the water outside the coastal zone} \\ & \text{or next to a land node} \\ 1, & \text{if the flux } V_{i,j} \text{ lies in a coastal zone, but not near a corner} \\ 0.5, & \text{if the flux } V_{i,j} \text{ lies in a coastal zone near a corner} \end{cases}$$

First the non-linear advection terms are calculated in every grid cell, using eq. (15) and (16). Then the terms are completed by approximation in the coastal zone using one of the four methods:

Method 1:

$$\widetilde{N}^x_{i,j\,(1)} = Z^x_{i,j}\, N^x_{i,j} \tag{17}$$

$$\widetilde{N}^y_{i,j\,(1)} = Z^y_{i,j}\, N^y_{i,j} \tag{18}$$

Method 2:

$$\widetilde{N}^x_{i,j\,(2)} = Z^x_{i,j}\, N^x_{i,j} + C^x_{i,j}\, (N^x_{i-1,j} + N^x_{i+1,j} + N^x_{i,j-1} + N^x_{i,j+1}) \tag{19}$$

$$\widetilde{N}^y_{i,j\,(2)} = Z^y_{i,j}\, N^y_{i,j} + C^y_{i,j}\, (N^y_{i-1,j} + N^y_{i+1,j} + N^y_{i,j-1} + N^y_{i,j+1}) \tag{20}$$

Method 3:

$$\begin{aligned} \widetilde{N}^x_{i,j\,(3)} = {} & Z^x_{i,j}\, N^x_{i,j} + \tfrac{1}{2} C^x_{i,j} [\ (2 - Z^x_{i-2,j})\, N^x_{i-1,j} + Z^x_{i-1,j}\, N^x_{i-2,j} \\ & + (2 - Z^x_{i+2,j})\, N^x_{i+1,j} + Z^x_{i+1,j}\, N^x_{i+2,j} \\ & + (2 - Z^x_{i,j-2})\, N^x_{i,j-1} + Z^x_{i,j-1}\, N^x_{i,j-2} \\ & + (2 - Z^x_{i,j+2})\, N^x_{i,j+1} + Z^x_{i,j+1}\, N^x_{i,j+2}\ ] \end{aligned} \tag{21}$$

$$\begin{aligned} \widetilde{N}^y_{i,j\,(3)} = {} & Z^y_{i,j}\, N^y_{i,j} + \tfrac{1}{2} C^y_{i,j} [\ (2 - Z^y_{i-2,j})\, N^y_{i-1,j} + Z^y_{i-1,j}\, N^y_{i-2,j} \\ & + (2 - Z^y_{i+2,j})\, N^y_{i+1,j} + Z^y_{i+1,j}\, N^y_{i+2,j} \\ & + (2 - Z^y_{i,j-2})\, N^y_{i,j-1} + Z^y_{i,j-1}\, N^y_{i,j-2} \\ & + (2 - Z^y_{i,j+2})\, N^y_{i,j+1} + Z^y_{i,j+1}\, N^y_{i,j+2}\ ] \end{aligned} \tag{22}$$

Method 4:

$$\begin{aligned}\widetilde{N}^x_{i,j\ (4)} = \ & Z^x_{i,j}\ N^x_{i,j} + C^x_{i,j}\,[\ (1+Z^x_{i-2,j})\ N^x_{i-1,j} - Z^x_{i-1,j}\ N^x_{i-2,j} \\ & +(1+Z^x_{i+2,j})\ N^x_{i+1,j} - Z^x_{i+1,j}\ N^x_{i+2,j} \\ & +(1+Z^x_{i,j-2})\ N^x_{i,j-1} - Z^x_{i,j-1}\ N^x_{i,j-2} \\ & +(1+Z^x_{i,j+2})\ N^x_{i,j+1} - Z^x_{i,j+1}\ N^x_{i,j+2}\ ]\end{aligned} \tag{23}$$

$$\begin{aligned}\widetilde{N}^y_{i,j\ (4)} = \ & Z^y_{i,j}\ N^y_{i,j} + C^y_{i,j}\,[\ (1+Z^y_{i-2,j})\ N^y_{i-1,j} - Z^y_{i-1,j}\ N^y_{i-2,j} \\ & +(1+Z^y_{i+2,j})\ N^y_{i+1,j} - Z^y_{i+1,j}\ N^y_{i+2,j} \\ & +(1+Z^y_{i,j-2})\ N^y_{i,j-1} - Z^y_{i,j-1}\ N^y_{i,j-2} \\ & +(1+Z^y_{i,j+2})\ N^y_{i,j+1} - Z^y_{i,j+1}\ N^y_{i,j+2}\ ]\end{aligned} \tag{24}$$

Note that for the fluxes in the water outside the coastal zone, eq. (17) to (24) become:

$$\widetilde{N}^x_{i,j\ (1)\to(4)} = \ N^x_{i,j} \qquad \widetilde{N}^y_{i,j\ (1)\to(4)} = \ N^y_{i,j}$$

since $Z^x_{i,j} = Z^y_{i,j} = 1$ and $C^x_{i,j} = C^y_{i,j} = 0$ in the water outside the coastal zone.

For our model setup the first and the last method proceed to be the most stable. Therefore section 5 only presents results from simulations with these two approximation methods.

Example A The flux, $V_{i,j}$, marked 'A' in figure 2 is located in the coastal zone, and has water outside the coastal zone, in one direction. Therefore the non-linear advection term is approximated in one direction. Eqs. (20), (22) and (24) become:

$$\begin{aligned}\widetilde{N}^y_{i,j\ (2)} &= N^y_{i-1,j} \\ \widetilde{N}^y_{i,j\ (3)} &= \frac{1}{2}(N^y_{i-1,j} + N^y_{i-2,j}) \\ \widetilde{N}^y_{i,j\ (4)} &= 2N^y_{i-1,j} - N^y_{i-2,j}\end{aligned}$$

Example B The flux, $U_{i,j}$, marked 'B' in figure 2 is located in the coastal zone near a corner. Since the flux has water outside the coastal zone in two directions, the non-linear advection term is approximated in these two directions. Eqs. (19), (21) and (23) become:

$$\begin{aligned}\widetilde{N}^x_{i,j\ (2)} &= \frac{1}{2}(N^x_{i+1,j} + N^x_{i,j+1}) \\ \widetilde{N}^x_{i,j\ (3)} &= \frac{1}{4}(N^x_{i+1,j} + N^x_{i+2,j} + N^x_{i,j+1} + N^x_{i,j+2}) \\ \widetilde{N}^x_{i,j\ (4)} &= \frac{1}{2}(2N^x_{i+1,j} - N^x_{i+2,j} + 2N^x_{i,j+1} - N^x_{i,j+2})\end{aligned}$$

Example C The flux, $V_{i,j}$, marked 'C' in figure 2 is located in the coastal zone, and has water outside the coastal zone, in one direction. The non-linear advection term is approximated in the same way as the flux in example A: Eqs. (20), (22) and (24) become:

$$\begin{aligned}
\widetilde{N}^y_{i,j\ (2)} &= N^y_{i,j+1} \\
\widetilde{N}^y_{i,j\ (3)} &= \frac{1}{2}(N^y_{i,j+1} + N^y_{i,j+2}) \\
\widetilde{N}^y_{i,j\ (4)} &= 2N^y_{i,j+1} - N^y_{i,j+2}
\end{aligned}$$

Example D The flux, $U_{i,j}$, marked 'D' in figure 4 is located in the coastal zone, and has water outside the coastal zone, in one direction. Since only one of the two nearest fluxes in that direction is located outside a coastal zone, only one grid cell is used in all the approximation methods. Eqs. (19), (21) and (23) become:

$$\widetilde{N}^x_{i,j\ (2)} = \widetilde{N}^x_{i,j\ (3)} = \widetilde{N}^x_{i,j\ (4)} = N^x_{i+1,j}$$

Example E The flux $U_{i,j}$, marked 'E' in figure 4 is located in the coastal zone, but does not have any neighbouring fluxes in water outside the coastal zone. Therefore this non-zero advection term is set to zero in all four approximation methods. Eqs. (19), (21) and (23) become:

$$\widetilde{N}^x_{i,j\ (2)} = \widetilde{N}^x_{i,j\ (3)} = \widetilde{N}^x_{i,j\ (4)} = 0$$

Example F The flux, $U_{i,j}$, marked 'F' in figure 4 is located in the coastal zone near a corner. Since the flux has water outside the coastal zone in two directions, the non-linear advection term is approximated in these two directions. In one of these direction, the flux two grid cells from the flux marked 'E' is located in a coastal zone. Eqs. (19), (21) and (23) become:

$$\begin{aligned}
\widetilde{N}^x_{i,j\ (2)} &= \frac{1}{2}(N^x_{i+1,j} + N^x_{i,j+1}) \\
\widetilde{N}^x_{i,j\ (3)} &= \frac{1}{4}(N^x_{i+1,j} + N^x_{i+2,j} + 2N^x_{i,j+1}) \\
\widetilde{N}^x_{i,j\ (4)} &= \frac{1}{2}(2N^x_{i+1,j} - N^x_{i+2,j} + N^x_{i,j+1})
\end{aligned}$$

3.3 Horizontal eddy viscosity

Following the same discretization as used in the original PLN-model, the horizontal eddy viscosities in eqs. (6) and (7) have the numerical form:

$$A^x_{i,j} = \frac{\nu}{(\triangle s)^2}(U_{i+1,j} + U_{i-1,j} + U_{i,j+1} + U_{i,j-1} - 4U_{i,j}) \quad (25)$$

$$A^y_{i,j} = \frac{\nu}{(\triangle s)^2}(V_{i+1,j} + V_{i-1,j} + V_{i,j+1} + V_{i,j-1} - 4V_{i,j}) \quad (26)$$

The PLN-model used in this report is without horizontal eddy viscosity. In order to make our non-linear simulations stable, sufficient horizontal eddy viscosity has to be included. This will be discussed further in section 5.1.

Since central differencing cannot be used in the coastal zone, the horizontal eddy viscosity cannot be calculated to the same order of accuracy in the coastal zone as in the interior domain. The four suggested approximation methods used for the non-linear advection terms, have also been evaluated for the eddy viscosity. The most stable method was to set the horizontal eddy viscosity to zero in the coastal zone. After calculating the various terms included in the horizontal eddy viscosity in the interior domain, the scheme is completed by setting these terms equal to zero in the coastal zone:

$$\widetilde{A}^x_{i,j} = Z^x_{i,j}\, A^x_{i,j}$$

$$\widetilde{A}^y_{i,j} = Z^y_{i,j}\, A^y_{i,j}$$

If the horizontal eddy viscosity is included closer than two grid cells from the FRS zone, the simulations become unstable in less than 20 hours simulated time. Therefore neither the horizontal eddy viscosity nor the non-linear advection terms are included closer than two grid cells from the FRS zone.

3.4 Bottom shear stress

According to Crean et al. (1995) the bottom shear stress dominates the horizontal eddy viscosity near the coast. Crean et al. therefore set the horizontal eddy viscosity to zero, and increased the bottom shear stress near the coast. We shall adopt a similar approach.

In order to improve the stability of the non-linear simulations we also found that the bottom shear stress coefficient has to be increased in the coastal zone. One way to increase the bottom shear stress in the coastal zone is simply to multiply the coefficient with a factor greater than unity. Another way to increase the bottom shear stress in the coastal zone, where

Color	Z	C	Description
Green	-	-	land nodes where $H_0 = 0$
	0	0	fluxes next to land nodes
Blue	-	-	water nodes where $H_0 > 0$
	1	0	fluxes in the water outside the coastal zone where eqs. 15 and 16, 25 and 26 are all used directly
Red	0	1	fluxes in the coastal zone
Yellow	0	0.5	fluxes in the coastal zone near a corner
Dotted	0	0	fluxes in the coastal zone where all non-linear terms are set to zero

Table 1: *Description of color codes in figure 2 and 4. Z represent Z^x and Z^y, and C represent C^x and C^y*

the water depths usually are small, is to assume that the bottom friction coefficient depends on the water depth:

$$c_D = c_D^0(1 + ae^{-\frac{H^2}{Hm^2}}) \tag{27}$$

where H is the water depth, H_m is a characteristic water depth in the coastal zone, $c_D^0 = 0.003$ is value of the coefficient in deep water ($H >> H_m$), and a is a positive scaling factor greater than unity.

In our simulations a suitable value of a was found to lie around five when the Smagorinsky formula, eq. (8) with $q = 0.3$, was used to calculate ν. When ν was constant, $\nu = 5m^2/s$, a was chosen around 15.

4 Model setup and boundary conditions

First the PLN-model with a 100 meter grid resolution was set up for a domain covering the Tjeldsund and Ramsund channels and the surrounding fjord areas as shown in figure 5. Boundary conditions in the FRS zone, ten grid cells wide, were obtained by interpolating surface elevation from the large-scale PLN-model for the area around the Lofoten Islands with 500 meter grid resolution (Moe et al. (2002)).

The high resolution depth matrix based on new bathymetric surveys of the model domain was not ready during this work. Therefore a test depth matrix with 100 meter grid grid resolution was constructed by interpolating from the depth matrix with 500 meter grid. Additional simulations will be conducted when a new depth matrix with 50 and 25 meter grid resolution becomes available.

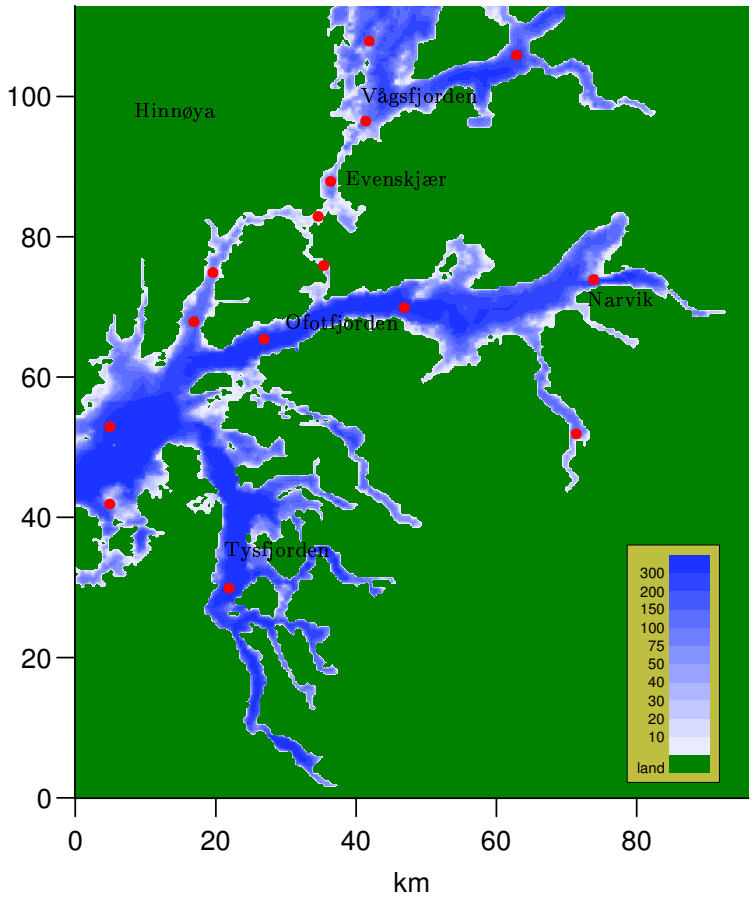

Figure 5: *The model domain covering the Tjeldsund and Ramsund channels and the surrounding fjord area. The red dots mark stations for output of time series.*

Next the PLN-model with a 100 meter grid resolution was set up for a sub domain covering only the Tjeldsund and Ramsund channels as shown in figure 6. The boundary conditions in the FRS zone were obtained from the model covering the whole domain in figure 5. The results of the simulations for the two model domains in figure 5 and 6 were compared. Only minor differences in the current and the surface elevation were detected.

Then the full non-linear model was set up for the domain in figure 6 with the same boundary conditions as for the PLN-model for the same domain. For the test depth matrix the mean water depth in the coastal zone, with special treatment of the non-linear advection terms, was 5.6 meters. The maximum water depth in the coastal zone was 29.5 meters. The reference depth H_m in eq. (27) was therefore set H_m=5.6 m.

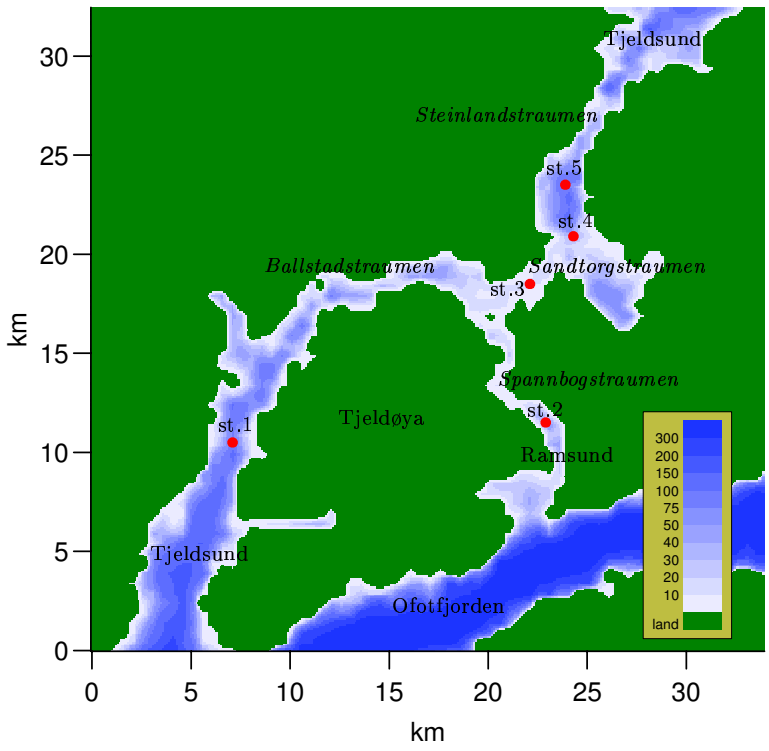

Figure 6: *The model domain for the full non-linear model. The red dots mark the five stations for output of time series, st.1 - st.5, discussed in this report.*

The tidal model reported here is driven only by surface amplitude and phase for the M_2 component at the open boundaries. The boundary forcing started from rest and increased in time with a ramping function, $(1 - \exp(-\sigma t))$. A value of $\sigma = 4.6 \times 10^{-5} s^{-1}$ has been used which implies full effect of boundary conditions after about 12 hours. This is similar to what was used for the PLN-model.

For every 180 seconds, surface elevation, current amplitude and phase at the output-stations were stored. Time series for the stations showed some noise due to the transient start. After 50 hours, full fields for current and elevation are stored every hour. A total simulation time of 100 hours seems to be sufficient to reach an acceptable steady state.

Two stations (st3, st4) in Sandtorgstraumen are of special interest. Both stations are marked with red dots in figure 11.

	ω	T	M_2	M_4	M_6	M_8
M_2	0.0805 cph	12.42 h	-	12.42 h	6.21 h	4.11 h
M_4	0.1610 cph	6.21 h	12.42 h	-	12.42 h	6.21 h
M_6	0.2415 cph	4.14 h	6.21 h	12.42 h	-	12.42 h
M_8	0.3220 cph	3.11 h	4.11 h	6.21 h	12.42 h	-

Table 2: *The frequents in cycles per hour (cph), the period of the tidal components, and the length of time series needed to separate the components by harmonic analysis.*

4.1 Harmonic analysis

To calculate the amplitude and phase for the tidal components the program T_TIDE (Pawlowicz et al. (2002)) was used with time series for surface elevation and depth mean current from the simulations as input. T_TIDE consists of a set of programs written in Matlab and uses classical harmonic analysis for periods of about 1 year or shorter. In classical harmonic analysis, the tidal signal is simulated as the sum of a finite set of sinusoidal components with specific frequencies determined from astronomical parameters for the orbits of the Moon and the Sun.

For the simulations reported here only the dominant M_2 component is used for boundary forcing. Due to non-linear effects the bottom friction generates the M_6 overtide with 4.1 hour period. The non-linear advection terms and the non-linearity in the eddy viscosity generates the M_4 and M_8 overtides with 6.2 and 3.1 hours period respectively.

The length of the time series needed to separate the component M_2 from M_4 by harmonic analysis is:

$$\frac{1}{\omega_4 - \omega_2} = 12.42 \text{ hours}$$

where ω_2 and ω_4 are the frequency in cycles per hour for M_2 and M_4 respectively.

Table 2 shows how long the time series must be, in order to separate some of the other tidal component.

5 Results

5.1 Currents and volume fluxes

Strong currents occur in Sandtorgstraumen north-east of Tjeldøya, in Steinlandsstraumen up north in Tjeldsundet and in Ballstadstraumen north of

		Bottom drag coefficient, c_D			
		depend on depths eq. 27		multiplied with n in coastal zone	
eddy viscosity coefficient, ν		$a = 2$	$a = 3$	$n = 4$	$n = 10$
constant	$\nu = 3$ m^2/s	unstable	unstable	unstable	unstable
	$\nu = 4$ m^2/s	-	-	-	stable
	$\nu = 5$ m^2/s	-	-	unstable	-
	$\nu = 6$ m^2/s	-	-	stable	-
	$\nu = 10$ m^2/s	-	unstable	-	-
	$\nu = 15$ m^2/s	unstable	stable	stable	stable
Smagorinsky	$q = 0.1$	unstable	unstable	unstable	unstable
eq. 8	$q = 0.2$	stable	stable	unstable	stable
	$q = 0.3$	-	-	stable	-
	$q = 5$	-	-	stable	-
	$q = 10$	stable	stable	unstable	stable

Table 3: *The stability after 100 hours of full non-linear simulations with different choices of friction coefficients, and the non-linear advection terms extrapolated in the coastal zone.*

Tjeldøya. In Spannbogstraumen in Ramsundet east of Tjeldøya the currents are weaker, but since the water depths are small and the channel is narrow, the currents is considerable even here.

Among the many difficulties with non-linear simulations, a crucial choice is to balance the amount of friction. With too little friction, the simulations become unstable, and too much friction, leads to an unrealistic strong damping of the current.

Table 3 shows which choices of ν and c_D that are suitable when the non-linear advection terms are extrapolated in the coastal zone. Note that when the Smagorinsky formula, eq. (8), is used to calculate the eddy viscosity coefficient, the simulations are stable only for an interval of q.

This section presents results from the five full non-linear simultions listed in table 4. For each of these simulations, the coefficients c_D and ν are chosen as small as possible for maintaining stabil solutions for 100 hours simulation time. If the coefficients are chosen smaller, the simulations become unstable. These limits depend on the topography, the grid length, location, initial conditions, boundary conditions, and current magnitude.

Figure 11 to 18 show plots which are generated from PLN-simulations and the five full non-linear simulations listed in tabel 4.

Figure 11 and 12 show the northern part of Sandtorgstraumen at the time

Run	Horizontal eddy viscosity coefficient	Bottom drag coefficient	Non-linear advection terms in coastal zone
1	$q = 0.3$ in eq. (8)	$a = 3$ in eq. (27)	extrapolated
2	$\nu = 6$ m^2/s, constant	x4 in coastal zone	extrapolated
3	$q = 0.3$ in eq. (8)	x4 in coastal zone	extrapolated
4	$\nu = 4$ m^2/s, constant	x4 in coastal zone	set to zero
5	$q = 0.1$ in eq. (8)		set to zero

Table 4: *The five full non-linear simulations.*

of maximum flow northwards. Figure 11 shows results from one PLN model simulation and the three full non-linear simulation where the non-linear advection terms are extrapolated in the coastal zone. Figure 12 shows results from the two full non-linear simulation where the non-linear advection terms are set to zero in the coastal zone. Plots from the same simulations are shown for maximum flow southwards in Sandtorgstraumen, and for Steinlandsstraumen in figure 13 to 18.

The most important differences between the simulations with the PLN-model and with the full non-linear model are the formation of intensified jets and eddies on various scales as shown in figure 11 to 18. Of course this is not unexpected, but we have been able to demonstrate how sensitive these current features are to various methods of implementing the non-linear advection terms.

All the simulations with the full non-linear model show an intensified jet flow and eddy structures on each side of the jet north-east of Sandtorgstraumen. The eddy structures have slightly different forms. A closer look at the plots from the full non-linear simulations reveals currents in the opposite direction close to land in some places. This effect is probably due to the increased bottom friction applied in the coastal zone. This effect is stronger when the non-linear advection terms are extrapolated in the coastal zone, compared to when the non-linear advection terms are set to zero.

When the non-linear advection terms are extrapolated in the coastal zone, and the horizontal friction coefficient, ν, is calculated using Smagorinsky formula, eq. (8), very strong currents occur close to land on the east side of the channel in the northern part of the domain as shown in figure 15b. These strong currents follow the coastal zone and are reflected at the northern boundary. These currents are most likely a result of the extrapolation since the magnitude is decreased when the non-linear advection terms are set to zero in the coastal zone.

Figure 7 displays the total volume flux through a cross-section in the middle of Sandtorgstraumen. The total volume flux at peak is up to 30%

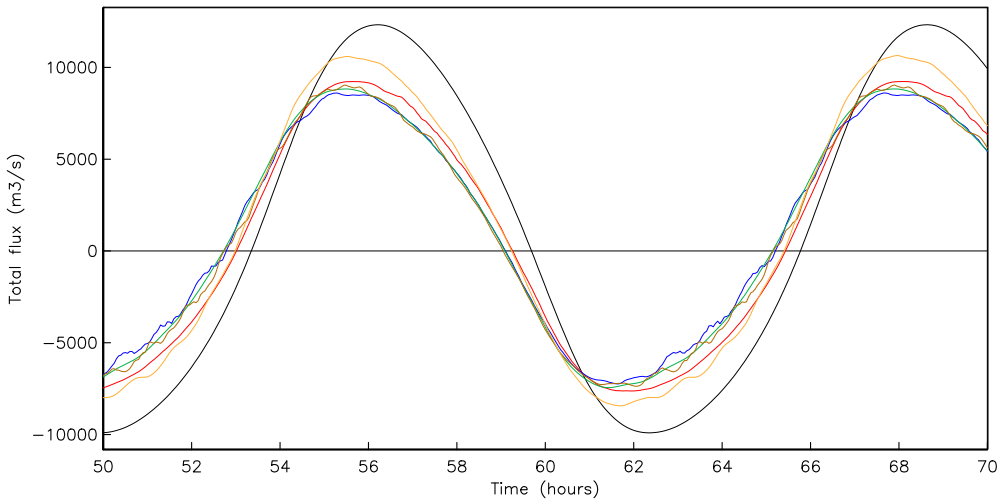

Figure 7: *Total volume flux through a cross-section in Sandtorgstraumen. The black line shows the result of the PLN-model. The other lines show results from the full non-linear simulations listed in table 4: Red line (run 1), blue line (run 2), green line (run 3), brown line (run 4), and orange line (run 5).*

smaller in full non-linear simulations compared to the PLN-model simulation. Since more friction is added in run 1-4 than in run 5, the total volume flux at peak in run 5 differ from the PLN-model simulation with less than 20%.

Figure 8 illustrates the impact of replacing H_0 with $H_0 + \eta$ in the PLN-model, compared with adding more friction in the PLN-model. The total volume flux at peak is decreased with up to 9% when $H_0 + \eta$ was used instead of H_0 in the PLN-model, and with up to 17 % when the friction of run 1 was added to the PLN-model.

5.2 Harmonic components

Figure 9 visualizes the currents at station 4. The currents vector calculated by the PLN-model follow a typical tide ellipse, but the variability calculated by the full non-linear model are more complicated. When T_TIDE is used to analyze the currents at station 4, it leads to a rather large rest current i.e. the difference between simulated currents and the currents T_TIDE recognizes as tidal currents. This is clearly seen from figure 10. The rest current is stable and periodic. The period of the rest current is from 1-4 hours and the amplitude is about 40 percent of the M_2 tidal component. The magnitude of the rest current vary much from one station to another.

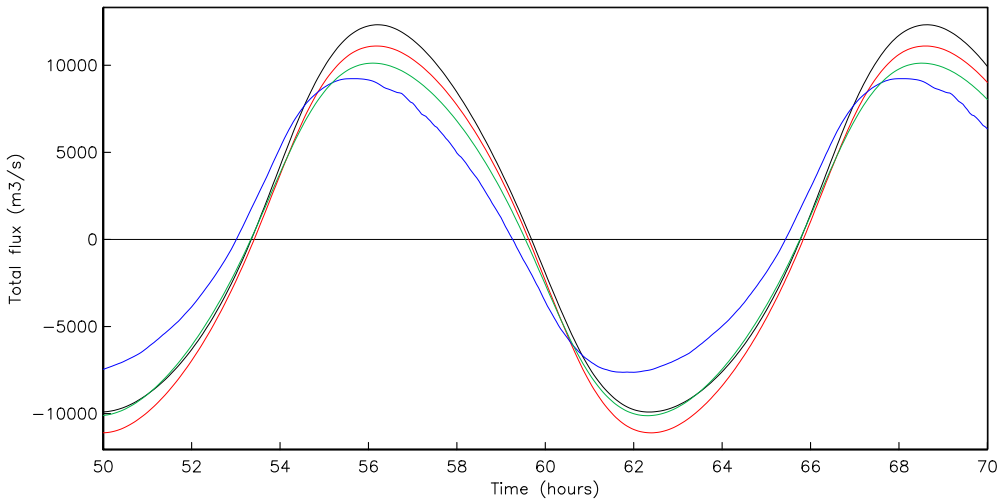

Figure 8: *Total volume flux through a cross-section in Sandtorgstraumen. The black line shows results of the PLN-model, and the red line shows results from the PLN-model modified with* $H = H_0 + \eta$ *instead of* H_0*. Both with constant bottom friction coefficient and no horizontal eddy viscosity.*
The blue line shows results from run 1 in table 4. The green line shows results from the PLN-model with the same friction choices as in the full non-linear simulation.

Table 5 and 6 show the calculated harmonic constants for the tidal components, sea level and current, for station 3 and 4. As the tables show, the amplitudes for M_4 and M_6 are, as expected, significantly larger in the full non-linear simulation compared to the PLN-simulation.

The observed sea level amplitude and phase for the actual tidal components (Lynge, 2004) are shown in table 7. Table 7 also shows results from the PLN-model, and table 8 shows results from the full non-linear model for the stations closest to the observed stations.

The simulated sea level amplitude for M_2 agrees well with the observed amplitude. The observed sea level amplitude for M_4 is somewhat larger than the simulated amplitudes. As expected the full non-linear model leads to larger amplitudes for M_4 than the PLN-model. The highest simulated sea level amplitude for M_4 is found when Smagorinsky formula is used instead of a constant eddy viscosity coefficient, and when the non-linear advection terms are extrapolated in the coastal zone, instead of setting these terms to zero in the coastal zone. The sea level amplitude for M_6 is larger for the full non-linear model than observed. This indicate that to much bottom friction is included.

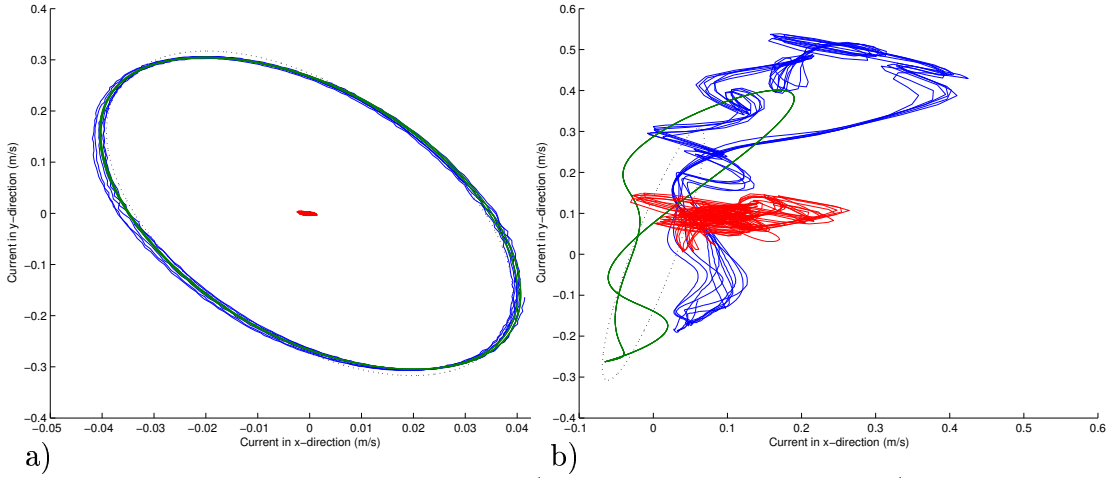

a) b)

Figure 9: *Currents at station 4 in a) a PLN-simulation, and b) the full non-linear simulation with run 5. The blue curve represents the simulated current, green the current that T_ Tide recognized as tide-currents, red represents the rest, and the dotted curve represents the tidal ellipse for* M_2.

6 Concluding remarks

Different strategies for including the non-linear advection terms in tidal simulations are tested and results of simulations are presented. Near the coast the non-linear advection terms can not be calculated with central differencing in the same manner as in the interior water. We have found that by extrapolating the non-linear advection terms into a narrow zone near the coast the simulations are less stable than when the non-linear advection terms are set to zero in this zone. Extrapolation leads however to stronger non-linear effects in the interior domain manifested by higher amplitudes of the overtides.

To make our full non-linear tidal simulations stable, sufficient horizontal eddy viscosity and bottom shear stress had to be included. If the non-linear advection terms are extrapolated in the coastal zone, a constant horizontal eddy viscosity coefficient of 6 m^2/s is proved to be sufficient if the bottom shear stress is increased by a factor of 4 near the coast. When the Smagorinsky formula is used for the horizontal eddy viscosity coefficient, a value of $q = 0.3$ is sufficient if the bottom stress coefficient either is increased four times near the coast or exponentially increased with depth with a factor $a = 3$, (eq. 27). If the non-linear advection terms are set to zero in the coastal zone, less friction need to be included. A constant horizontal eddy viscosity coefficient of 4 m^2/s is proved to be sufficient if the bottom stress coefficient is increased by a factor of 4 near the coast. And when the Smagorinsky formula is used for the horizontal eddy viscosity coefficient, a

st 3	PLN-model		Full non-linear (run 5)	
const.	h_η [cm]	g_η [deg]	h_η [cm]	g_η [deg]
M_2	83.94 ± 0.001	339.68 ± 0.05	84.94 ± 0.000	4.43 ± 0.03
M_4			1.60 ± 0.000	205.42 ± 1.24
M_6	0.64 ± 0.001	49.77 ± 7.32	0.85 ± 0.000	109.56 ± 2.41

st 4	PLN-model		Full non-linear (run 5)	
const.	h_η [cm]	g_η [deg]	h_η [cm]	g_η [deg]
M_2	74.20 ± 0.000	340.27 ± 0.04	75.11 ± 0.000	5.79 ± 0.01
M_4			0.50 ± 0.000	347.40 ± 1.85
M_6	0.67 ± 0.000	122.80 ± 3.82	1.04 ± 0.000	160.95 ± 0.99

Table 5: *The calculated harmonic constants for see level amplitude, h_η, and phase relative Greenwich, g_η, at station 3 and 4.*

value of $q = 0.1$ is sufficient without increasing the bottom stress coefficients.

We advice to set the non-linear advection terms to zero in a narrow zone near the coast, use Smagorinsky formula to calculate the horizontal eddy viscosity coefficient, and, if necessary, increase the bottom stress coefficient exponentially with depth (eq. 27). Note that when the Smagorinsky formula is used for the horizontal eddy viscosity coefficient, and sufficient bottom shear stress is included, the simulations are stable only for an interval of q.

For the 100 meter grid used here depth is interpolated from a depth matrix with 500 meter grid. More simulation tests will be conducted when a new depth matrix with grid resolution of 25 and 50 meter is constructed from new bathymetric data.

When a full non-linear simulation is run with a new depth matrix we expect that the coefficients of both the bottom friction and the horizontal eddy viscosity have to be modified in order to make the simulations stable with a realistic amount of damping. The results presented in this report provide a guidance for how friction has to be adjusted.

st 3	PLN-model				Full non-linear (run 5)			
const.	A [cm/s]	B [cm/s]	θ [deg]	g_c [deg]	A [cm/s]	B [cm/s]	θ [deg]	g_c [deg]
M_2	118.8	-3.9	27.1	28.4	115.3	-0.5	28.3	18.3
M_4					6.6	-0.3	21.1	16.3
M_6	6.0	-1.0	20.4	339.6	8.0	-0.6	18.2	305.2
M_8					0.7	-0.4	32.7	307.4

st 4	PLN-model				Full non-linear (run 5)			
const.	A [cm/s]	B [cm/s]	θ [deg]	g_c [deg]	A [cm/s]	B [cm/s]	θ [deg]	g_c [deg]
M_2	32.1	-3.4	93.5	46.7	35.3	3.0	76.5	29.0
M_4					9.0	2.5	46.9	43.1
M_6	0.13	-0.1	94.0	335.6	7.0	-0.1	27.3	34.3
M_8					3.9	0.9	24.1	23.8

Table 6: *The calculated parameters of current ellipse at station 3 and 4. Major and minor half axis denoted A and B respectively. Orientation, θ, of major axis relative east, and phase, g_c, degrees relative Greenwich, (east: $g_c = 0^o$, south: $g_c = 0^o$, etc.).*

References

P.B. Crean, T.S. Murty, and J.A. Stronach. Mathematical Modelling of Tides and Estuarine Circulation. *Springer-Verlag, N.Y.*, 1988

B. Gjevik. Model simulations of tides and shelf waves along the shelves of the Norwegian-Greenland-Barents Seas. *Modelling Marine Systems*, Vol.I, p. 187-219. Ed. A.M. Davies, CRC Press Inc. Boca Raton, Florida, 1990.

B. Gjevik, E. Nøst, T. Straume. Model simulations of the tides in the Barents Sea. *J. Geophysical Res.*, Vol. 99, No C2, 3337–3350, 1994.

B. Gjevik, D. Hareide, B.K. Lynge, A. Ommundsen, J.H. Skailand, and H.B. Urheim. Implementation of high resolution tidal current fields in electronic navigational chart systems. *Preprint Series,* Department of Mathematics, University of Oslo. ISSN 0809-4403, 2004.

B.K. Lynge Water level observations from Tjeldsundet. January-March 2004. *Norwegian Hydrographic Service,* report nr. DAF 04-2, 2004.

E.A. Martinsen, and H. Engedahl. Implementation and testing of a lateral

OBSERVED	M_2		M_4		M_6	
	h [cm]	g [deg]	h [cm]	g [deg]	h [cm]	g [deg]
Lødingen	96.3	334.1	4.8	276.2	0.9	341.9
Ramsund	97.9	334.3	5.2	276.4	1.0	346.7
Fjelldal	87.5	340.0	2.5	285.1	0.7	4.1
Evenskjær	73.7	341.2	1.2	251.1	0.3	36.3
PLN-MODEL with $c_D = 0.03$, $\nu = 0$						
station 1	95.8	335.4	-	-	-	-
station 2	97.6	335.6	-	-	-	-
station 3	83.9	339.7	-	-	0.6	49.8
station 4	74.2	340.3	-	-	0.7	122.8
station 5	73.8	340.6	-	-	0.7	118.9

Table 7: *Observed and simulated amplitude and phase for sea level (PLN-model). Lødingen is located near station 1, Ramsund is located near station 2, Fjelldal near station 3, and Evenskjær is located between station 4 and 5.*

boundary scheme as an open boundary condition in a barotropic ocean model. *Coastal Engineering,* Vol. 11, 603–627, 1987.

F. Mesinger, and A. Arakawa. Numerical Methods Used in Atmospheric Models. *GARP Publications Series,* No.17. 64pp, 1976.

H. Moe, A. Ommundsen, and B. Gjevik. A high resolution tidal model for the area around the Lofoten Islands, Northern Norway. *Continental Shelf Research 22*, 485-504, 2002.

H. Moe, B. Gjevik, and A. Ommundsen. A high resolution tidal model for the coast of Møre and Trøndelag, Mid-Norway. *Norwegian journal of Geography,* Vol. 57, 65-82. Oslo. ISSN 0029-1951, 2003.

S. Orre, E. Åkervik, and B. Gjevik. Analysis of current and sea level observations from Trondheimsleia. *Preprint Series*, Department of Mathematics, University of Oslo. ISSN 0809-4403, 2004.

R. Pawlowicz, B. Beardsley, and S. Lentz. Classical Tidal Harmonic Analysis Icluding Error Estimated in MATLAB using T_TIDE. *Computers and Geosciences*, 28, 929-937, 2002.

J. Smagorinsky. General circulation experiments with the primitive equations. *Monthly Rewiew* 91 (1), 99-164, 1963.

SIMULATED	M_2		M_4		M_6	
full non-linear	h [cm]	g [deg]	h [cm]	g [deg]	h [cm]	g [deg]
Run 1						
station 1	96.2	335.4	-	-	-	-
station 2	83.0	341.7	4.3	157.1	1.4	16.7
station 3	86.9	340.6	2.5	160.7	1.3	9.7
station 4	76.9	342.5	1.6	216.8	1.7	63.3
station 5	76.8	342.5	1.6	212.8	1.7	64.5
Run 2						
station 1	96.1	335.4	-	-	0.1	311.4
station 2	97.5	335.7	-	-	0.1	270.2
station 3	85.1	340.5	1.9	156.0	1.1	30.6
station 4	76.2	342.2	0.6	247.9	1.4	67.1
station 5	76.0	342.3	0.6	253.2	1.3	65.2
Run 3						
station 1	96.2	335.4	-	-	-	-
station 2	97.8	335.5	-	-	-	-
station 3	85.5	340.5	2.1	157.4	1.1	29.5
station 4	76.4	342.2	1.0	219.9	1.4	69.2
station 5	76.2	342.2	0.9	229.5	1.4	65.7
Run 4						
station 1	96.1	335.4	-	-	-	-
station 2	97.5	335.7	-	-	-	-
station 3	84.8	340.4	1.7	151.8	1.0	36.9
station 4	76.2	342.1	0.4	257.4	1.2	69.4
station 5	76.1	342.3	0.3	286.1	1.3	98.0
Run 5						
station 1	96.1	359.8	0.1	111.4	1.3	25.3
station 2	75.4	5.8	0.4	359.9	1.3	157.1
station 3	84.9	4.4	1.6	205.4	0.8	109.6
station 4	75.1	5.8	0.5	347.4	1.0	160.1
station 5	75.1	5.7	0.5	342.1	1.1	164.0

Table 8: *Simulated amplitude and phase for sea level from the full non-linear model. For further explanations see legend table 7*

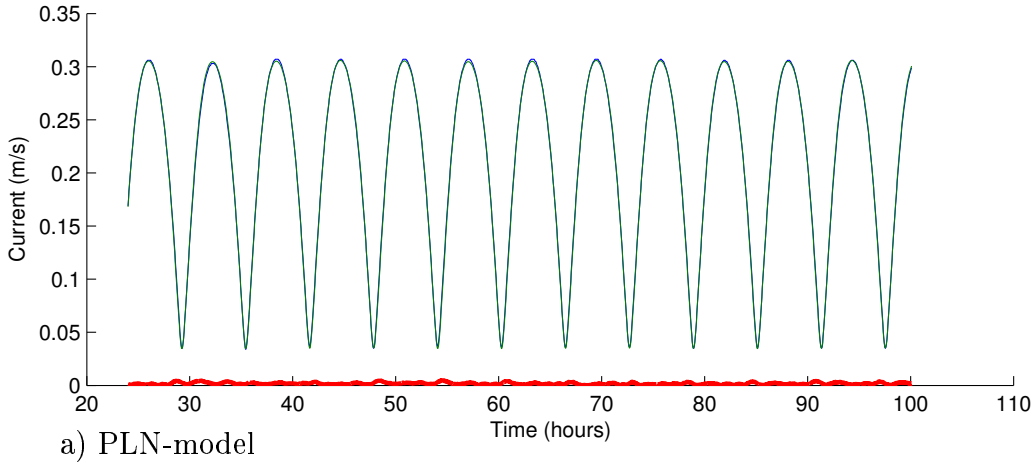

a) PLN-model

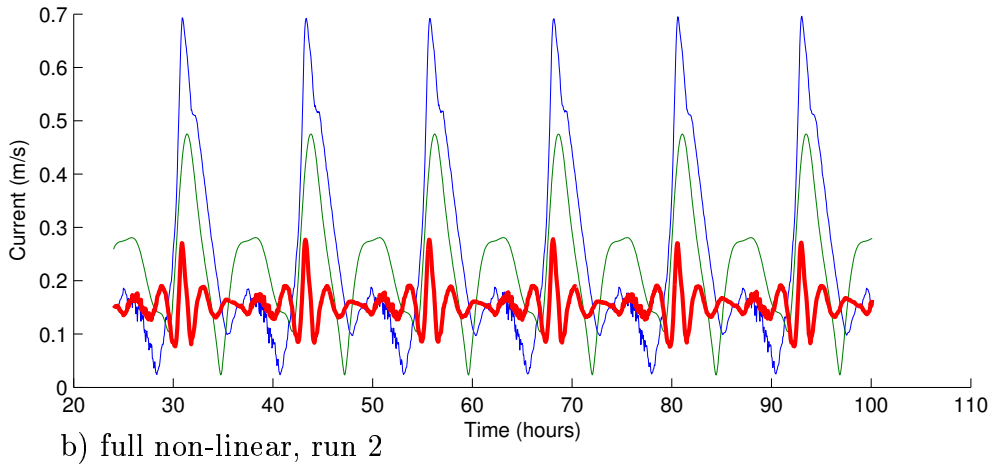

b) full non-linear, run 2

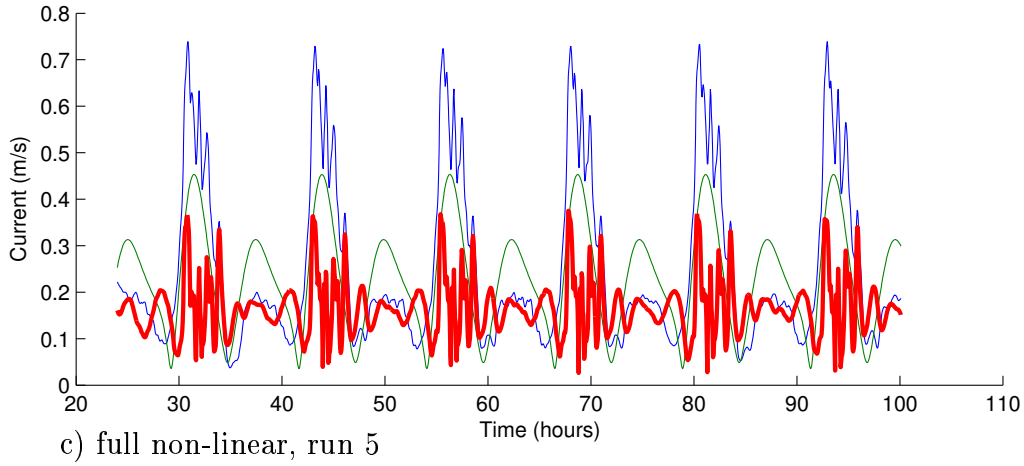

c) full non-linear, run 5

Figure 10: *Harmonic analysis of the current at station 4. The blue curve represents the simulated current, green the current that T_Tide recognized as tide-currents and red the rest current.*

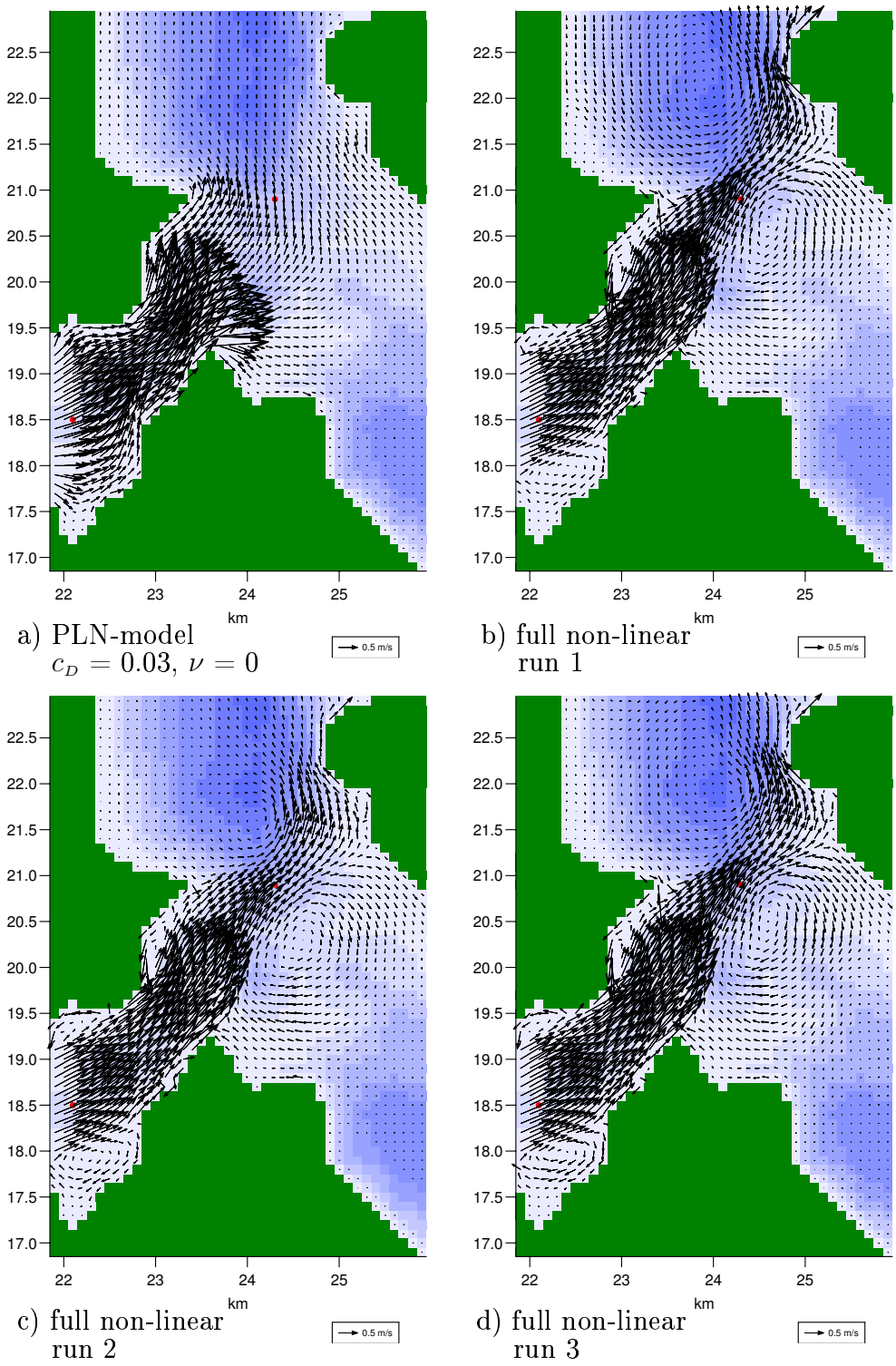

a) PLN-model
$c_D = 0.03$, $\nu = 0$

b) full non-linear
run 1

c) full non-linear
run 2

d) full non-linear
run 3

Figure 11: *Maximum flood currents northwards in Sandtorgstraumen when the non-linear advection terms are extrapolated in the coastal zone .*

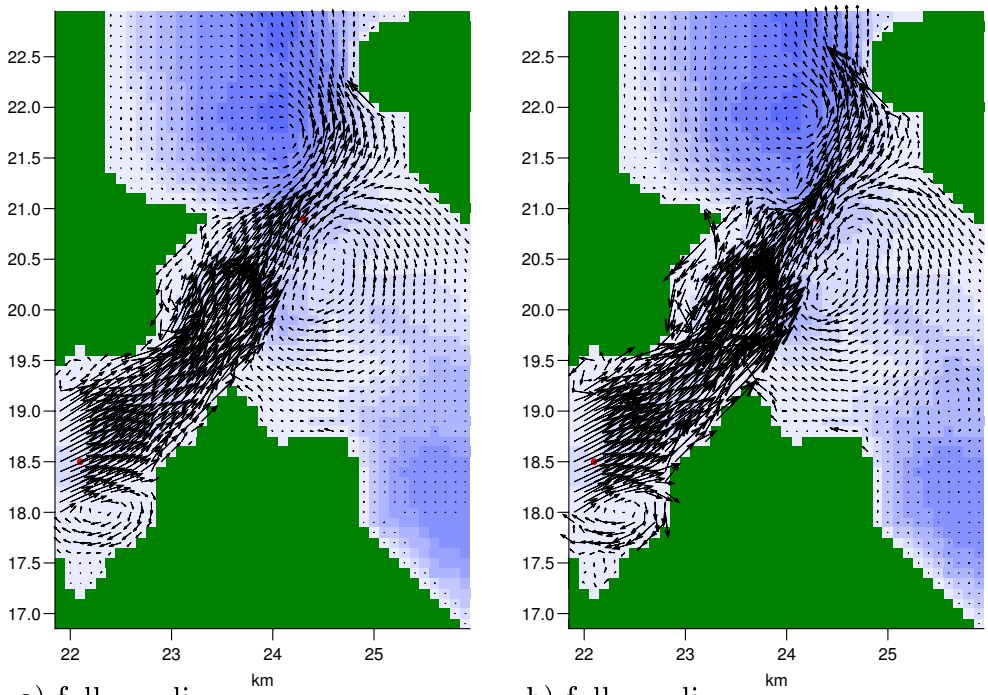

a) full non-linear run 4

b) full non-linear run 5

Figure 12: *Maximum flood currents northwards in Sandtorgstraumen when the non-linear advection terms are set to zero in the coastal zone.*

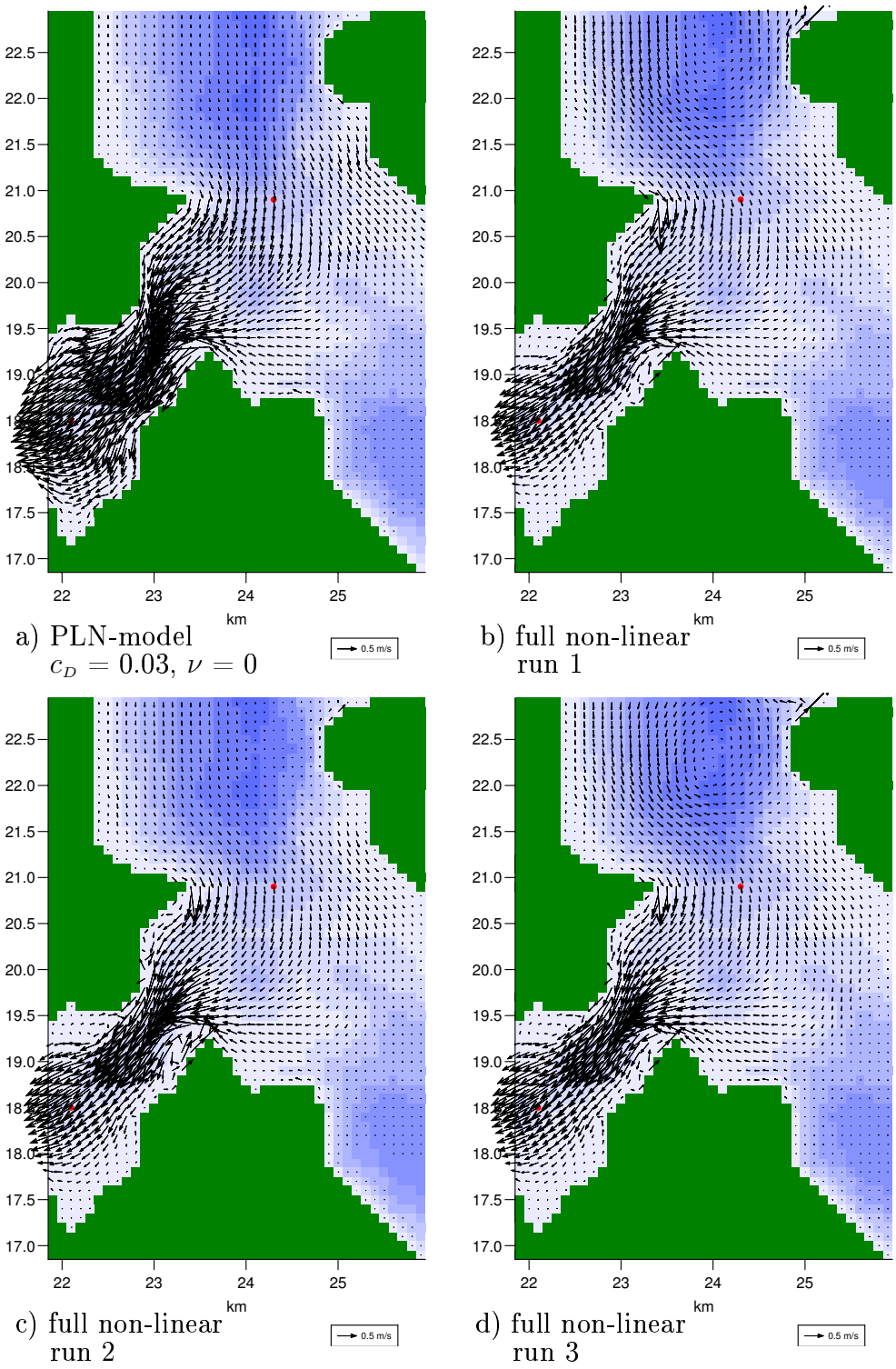

a) PLN-model
$c_D = 0.03$, $\nu = 0$

b) full non-linear
run 1

c) full non-linear
run 2

d) full non-linear
run 3

Figure 13: *Maximum ebb currents southwards in Sandtorgstraumen when the non-linear advection terms are extrapolated in the coastal zone.*

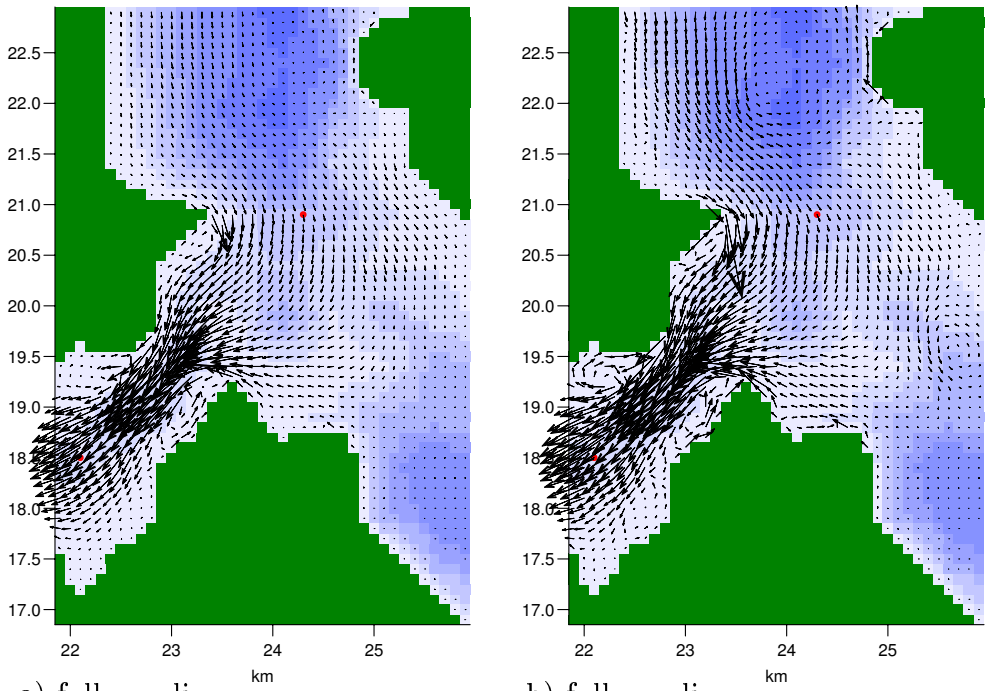

a) full non-linear run 4

b) full non-linear run 5

Figure 14: *Maximum ebb currents southwards in Sandtorgstraumen when the non-linear advection terms are set to zero in the coastal zone.*

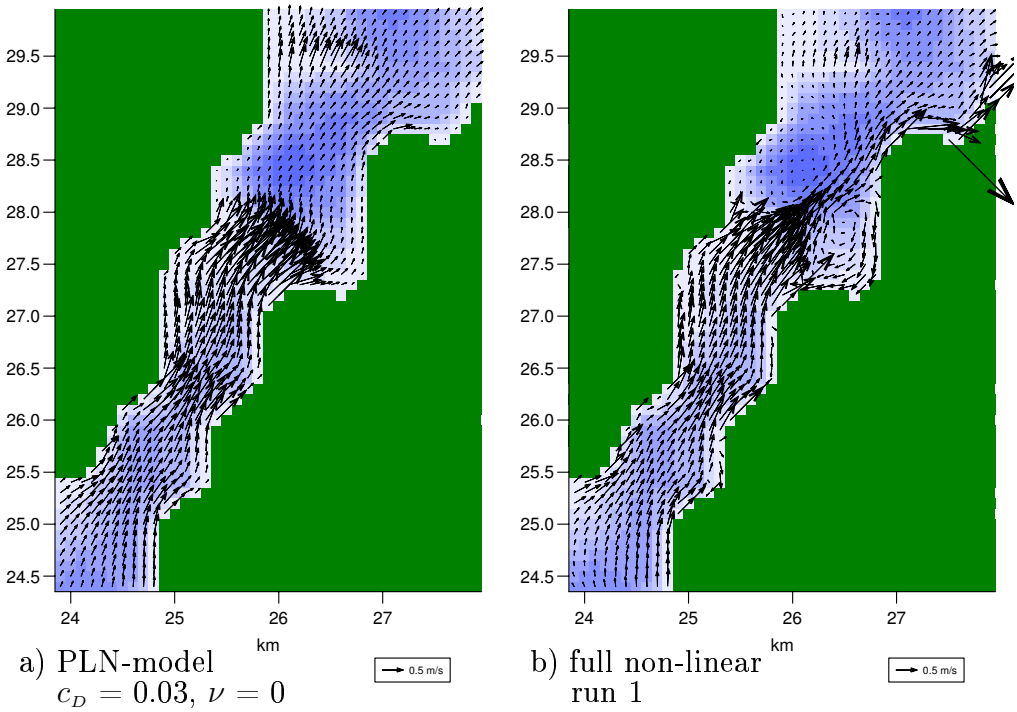

a) PLN-model
$c_D = 0.03$, $\nu = 0$

b) full non-linear
run 1

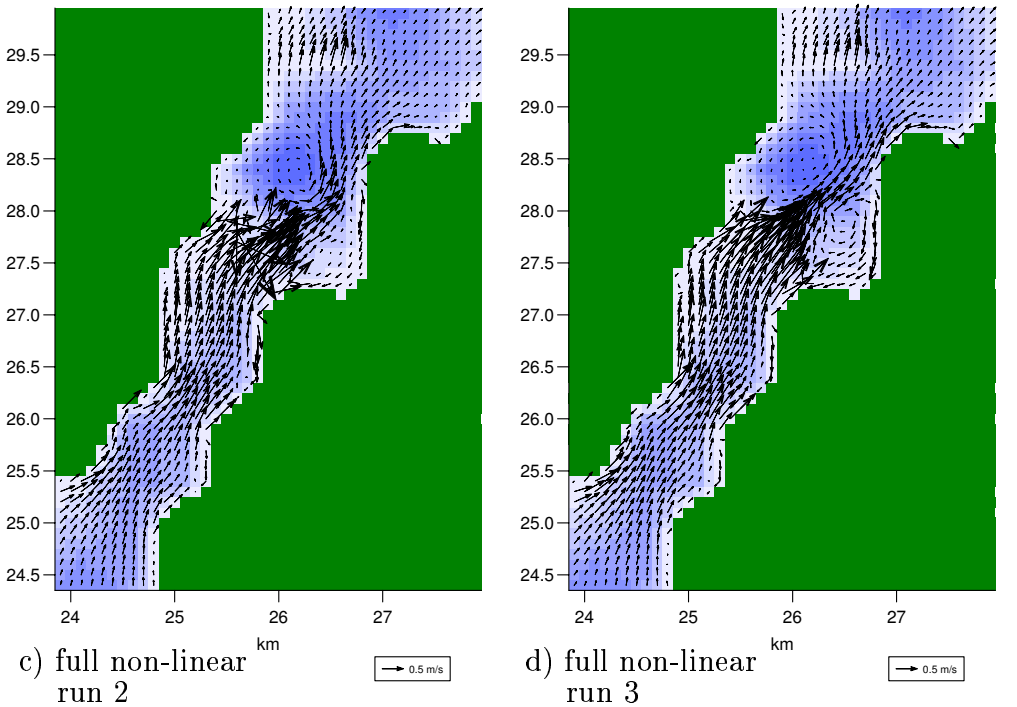

c) full non-linear
run 2

d) full non-linear
run 3

Figure 15: *Maximum flood currents northwards in Steinlandstraumen when the non-linear advection terms are extrapolated in the coastal zone.*

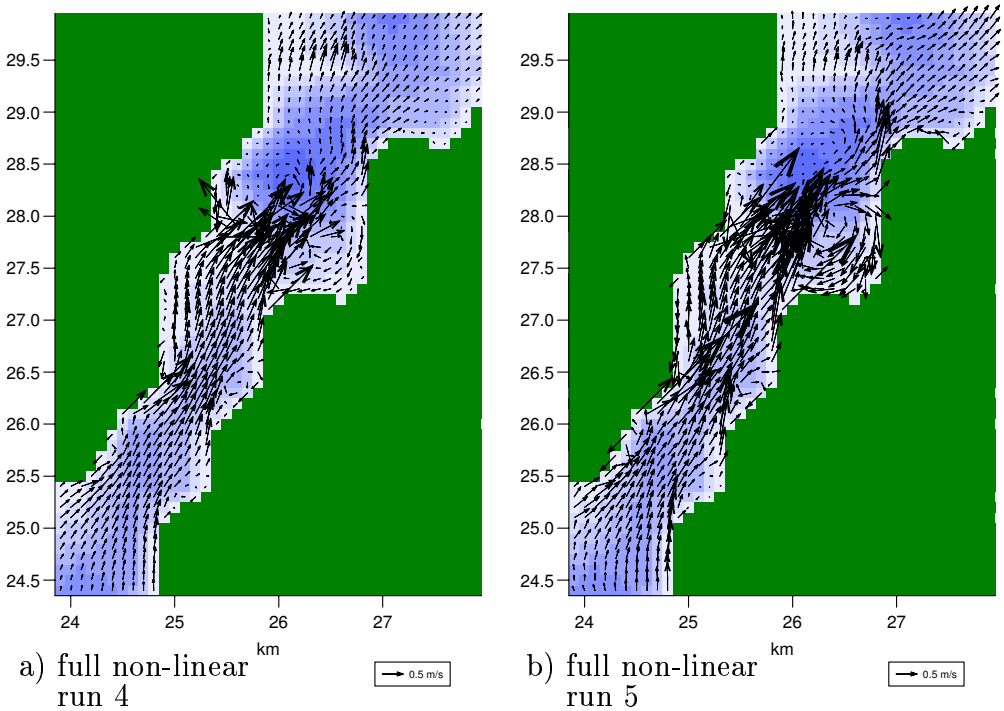

a) full non-linear run 4

b) full non-linear run 5

Figure 16: *Maximum flood currents northwards in Steinlandstraumen when the non-linear advection terms are set to zero in the coastal zone.*

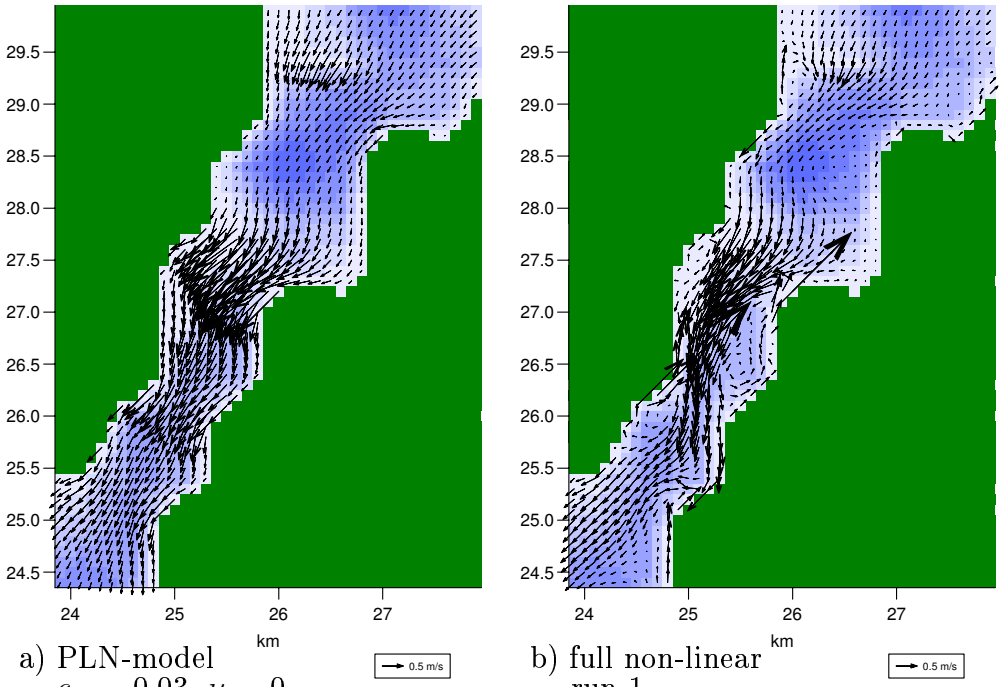

a) PLN-model
$c_D = 0.03$, $\nu = 0$

b) full non-linear
run 1

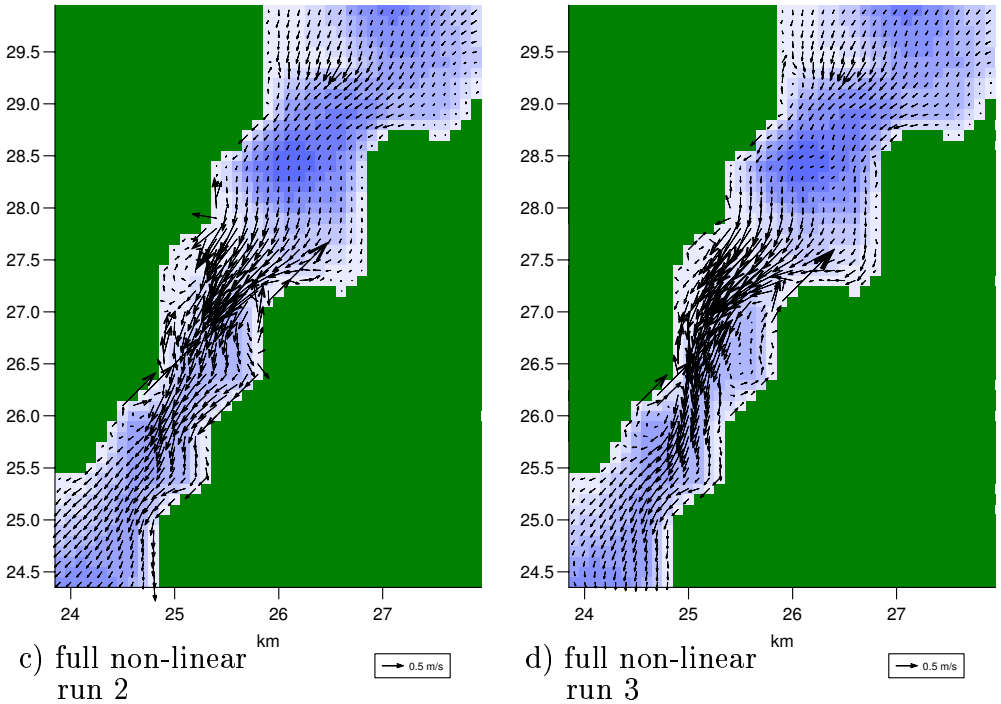

c) full non-linear
run 2

d) full non-linear
run 3

Figure 17: *Maximum ebb currents southwards in Steinlandstraumen when the non-linear advection terms are extrapolated in the coastal zone.*

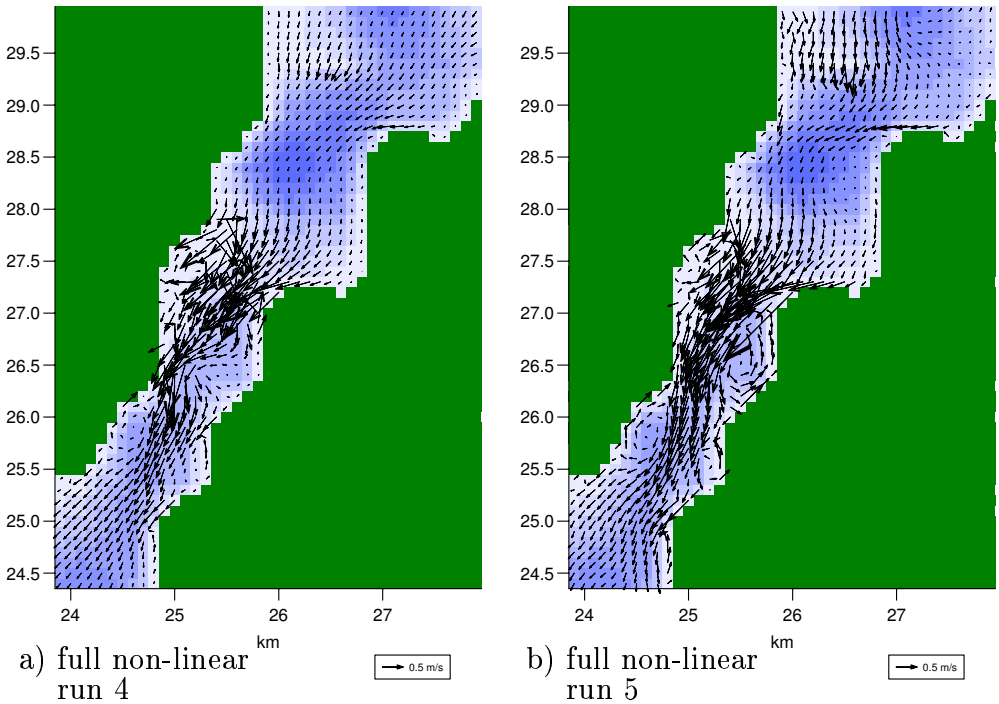

a) full non-linear run 4

b) full non-linear run 5

Figure 18: *Maximum ebb currents southwards in Steinlandstraumen when the non-linear advection terms are set to zero in the coastal zone.*